TimewarpVAE: Simultaneous Time-Warping and Representation Learning of Trajectories

Travers Rhodes and **Daniel D. Lee**
Cornell Tech
New York, NY 10044, USA
{tsr42,ddl46}@cornell.edu

Abstract

Human demonstrations of trajectories are an important source of training data for many machine learning problems. However, the difficulty of collecting human demonstration data for complex tasks makes learning efficient representations of those trajectories challenging. For many problems, such as for dexterous manipulation, the exact timings of the trajectories should be factored from their spatial path characteristics. In this work, we propose TimewarpVAE, a fully differentiable manifold-learning algorithm that incorporates Dynamic Time Warping (DTW) to simultaneously learn both timing variations and latent factors of spatial variation. We show how the TimewarpVAE algorithm learns appropriate time alignments and meaningful representations of spatial variations in handwriting and fork manipulation datasets. Our results have lower spatial reconstruction test error than baseline approaches and the learned low-dimensional representations can be used to efficiently generate semantically meaningful novel trajectories. We demonstrate the utility of our algorithm to generate novel high-speed trajectories for a robotic arm.

1 Introduction

Continuous trajectories are inherently infinite-dimensional objects that can vary in complex ways in both time and space. However, in many practical situations, their intrinsic sources of variability can be well-approximated by projection onto a low-dimensional manifold. For instance, when a human demonstrates trajectories for a robot, it is useful for the robot to learn to model the most expressive latent factors controlling the functionally-relevant parts of the demonstration trajectories. For many types of demonstrations, such as in gesture control or quasistatic manipulation, it is highly advantageous to explicitly separate the exact timing of the trajectory from the spatial latent factors. This work introduces a method that learns such a representation to generate novel fast trajectories for a robot arm, as shown in Fig 1.

Consider the problem of trying to average two samples from a handwriting dataset generated by humans drawing the letter "A" in the air [Chen *et al.*, 2012]. If we scale two trajectories linearly in time so that their timestamps go from 0 to 1, and then average the two trajectories at each timestep, the resulting average does not maintain the style of the "A"s. This is because the average is taken between parts of the two trajectories that do not naturally correspond. An example of this averaging, with lines showing examples of averaged points, is shown in Fig. 2a. Scaling trajectories to have constant speed also doesn't solve the issue (Fig. 2b). A common approach like dynamic time warping (DTW) [Sakoe and Chiba, 1978] can lead to unintuitive results. When averaging these same two trajectories, DTW only takes in information about these two trajectories and does not use contextual information about other examples of the letter "A" to better understand how to align the timings of these trajectories.[1] In Fig. 2c, we use the `dtw` package [Giorgino, 2009] to align the trajectories before averaging them at corresponding timesteps. We see the resulting trajectory is spatially close to the input trajectories, but it again does not maintain the style of the "A"s.

Our TimewarpVAE takes the time alignment benefits of DTW and uses them in a manifold learning algorithm to align the timings of similar trajectories. Our results are shown in Fig. 2e. The Rate Invariant Autoencoder of [Koneripalli *et al.*, 2020] is similar in also learning a latent space that separates timing and spatial factors of variation, with the spatial inter-

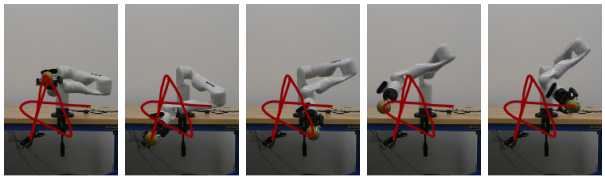

Figure 1: TimewarpVAE learns a low-dimensional latent representation of complex trajectories that explicitly factorizes timing and spatial styles. The Kinova Gen3 robot arm is able to draw various versions of the letter "A" more quickly by speeding up or slowing down different parts of the trajectory to obey dynamical mechanical constraints. The resulting end-effector path is overlaid on the images. A video and more details are provided in the Supplemental Materials.

[1] We use the terms "time-warping," "time alignment," and "registration" interchangeably.

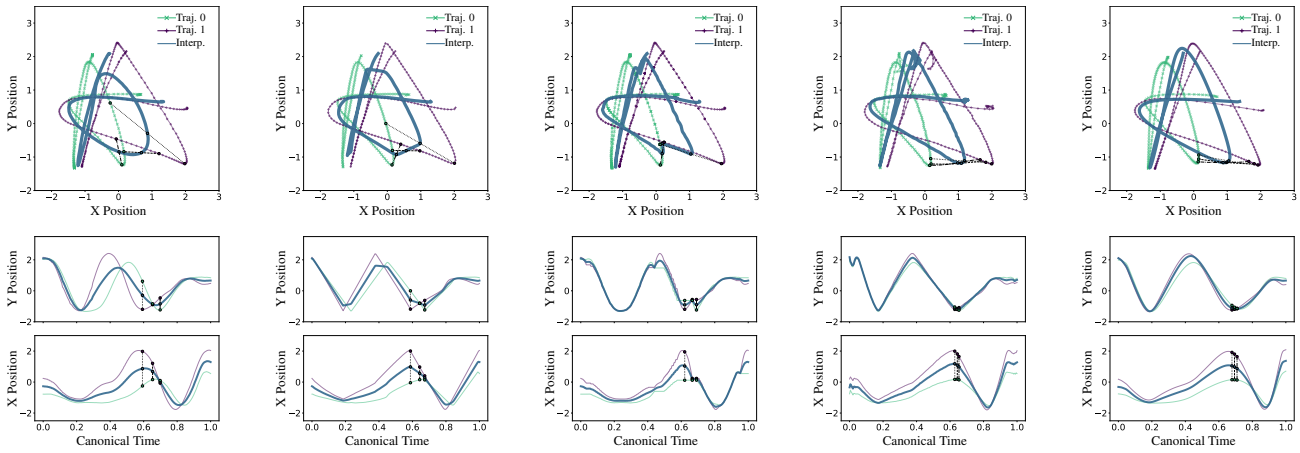

(a) Uniform time scaling (b) Constant speed scaling (c) DTW time alignment (d) Rate Invariant AE (e) TimewarpVAE (ours)

Figure 2: Interpolations in latent space between canonical trajectories using various models. For Rate Invariant Autoencoder and TimewarpVAE, we use a sixteen dimensional spatial latent space and the interpolation is constructed by decoding the average of the spatial latent embeddings. The resulting average trajectory is plotted alongside the reconstructions of the original two trajectories. The Rate Invariant Autoencoder can ignore parts of the canonical trajectory during training, leading to the jittering seen at the beginning and end of the canonical trajectory.

polations shown in Fig. 2d. Our TimewarpVAE approach has three main contributions that make it better suited for generating robot trajectories than a Rate Invariant AE. The first is the parameterization of the generated trajectory as an arbitrarily complicated neural network function of time rather than basing the trajectory calculation on piecewise linear functions with a pre-specified number of knots. The second is that our approach includes a regularization term, so the model is correctly penalized for extreme time warps. Finally, because of our time-warping regularization term, a robot can optimize the trajectory timing to account for its own joint torque and speed limitations, speeding up its execution of learned trajectories while regularizing to stay close to training timings. An example optimized trajectory is shown in Fig 1.

2 Related Work

Learning a latent space of trajectories that combines the timing and spatial parameters together into a single latent space appears in [Coll-Vinent and Vondrick, 2022], [Chen *et al.*, 2021], and [Lu *et al.*, 2019], among others. TimewarpVAE, like the Rate Invariant Autoencoder of [Koneripalli *et al.*, 2020], instead separates the timing and spatial latent variables, giving a more efficient spatial model. Our work is an improvement over the Rate Invariant AE in two important ways. First, our work is not constrained to learning a piecewise linear trajectory. Second, we include a proper regularization term to penalize the time warping so it does not ignore parts of the template trajectory. Comparing our results to the Rate Invariant AE shows that this timing regularization is important to combat a degeneracy in the choice of timing of the canonical trajectory. We explain this degeneracy in Section 4.1 and explain how it also applies to the work of [Shapira Weber *et al.*, 2019] in the Appendix.

Functional Data Analysis [Wang *et al.*, 2016] involves the study of how to interpret time-series data, often requiring the registration of data with different timings. The idea of warping the timings of paths appears in, for example, DTW [Sakoe and Chiba, 1978] and the Fréchet distance [Fréchet, 1906]. Our work is also related to continuous dynamic time warping [Kruskal and Liberman, 1983], which we refine for the manifold-learning setting. The registration and averaging of trajectories is performed in [Petitjean *et al.*, 2011], [Schultz and Jain, 2018], and [Williams *et al.*, 2020]. Rather than just learning a single average trajectory, we model the full manifold of trajectories. Time-warping is used in [Chang *et al.*, 2021] to learn "discriminative prototypes" of trajectories, but not a manifold representation of all the trajectories. A linear model to give a learned representation of registered trajectories is generated in [Kneip and Ramsay, 2008], and our work can be considered an expansion of that work, using manifold learning to allow for nonlinear spatial variations of registered trajectories.

Time-warping has previously been combined with manifold learning to generate representations of individual frames of a trajectory. For example, [Zhou and la Torre, 2012], [Trigeorgis *et al.*, 2018], and [Cho *et al.*, 2023] align trajectories and learn representations of individual frames contained in the trajectories. Connectionist Temporal Classification (CTC) can also be viewed as an algorithm for learning a labeling of frames of a trajectory while ignoring timing variations [Graves *et al.*, 2006]. Instead, our approach focuses on learning a latent vector representation that captures information about the entire trajectory.

Trajectory data can be parameterized in many ways when presented to the learning algorithm. For example, the trajectory could be parameterized as a dynamic movement primitive (DMP) [Ijspeert *et al.*, 2013] before learning a (linear) model of DMP parameters, as is done in [Matsubara *et al.*, 2011]. A DMP can also be used to learn a representation of states [Chen *et al.*, 2016] and to model trajectories; for ex-

ample, the timing can be slowed during execution to allow a robot to "catch up" and correct for execution errors [Schaal *et al.*, 2007]. However, that work does not model timing variations during training. We find the Parametric DMP model is not as accurate as TimewarpVAE. TimewarpVAE accounts for timing variations during training, enabling its latent variable to concentrate its modeling capacity on spatial variations of trajectories.

3 Technical Approach

A standard approach to learning a manifold for trajectories (see, for example the method proposed by [Chen and Müller, 2012]) is to map each trajectory to a learned representation that includes information about timing and spatial variations. This type of representation learning can be performed by a beta-Variational Auto-Encoder (beta-VAE) [Higgins *et al.*, 2017]. We provide a brief introduction to beta-VAE for comparison with our TimewarpVAE.

3.1 Beta-VAE

A beta-VAE encodes each datapoint x into a learned probability distribution $q(z|x)$ in the latent space and decodes points in the latent space into probability distributions $p(x|z)$ in the data space. A standard formulation of beta-VAE is to parameterize the encoder distributions as axis-aligned Gaussians $q(z|x) = \mathcal{N}(e(x), \sigma^2(x))$. Thus, the encoder returns the expected latent value $z = e(x) \in \mathbb{R}^\ell$ for a trajectory, along with the log of the (diagonal) covariance of the encoder noise distribution given by $\log(\sigma^2) \in \mathbb{R}^\ell$. For continuous data, we constrain the decoder distribution to have spherical covariance with diagonal elements all equal to some constant (not-learned) value σ_R^2. Thus, the decoder f only needs to return the expected decoded trajectory $\tilde{x}$, given a latent value. The beta-VAE architecture is shown in Fig. 3. Its loss function is $\mathcal{L} = \mathcal{L}_R + \mathcal{L}_{\text{KL}}$, where

$$\mathcal{L}_R = \frac{1}{\sigma_R^2}\mathbb{E}_{x_i,t,\epsilon}\left[\left\|x_i(t) - f\left(e(x_i) + \epsilon\right)_t\right\|^2\right] \tag{1}$$

$$\mathcal{L}_{\text{KL}} = \beta\mathbb{E}_{x_i}\left[\frac{\|e(x_i)\|^2 + \sum_d(\sigma_d^2(x_i) + \log(\sigma_d^2(x_i)))}{2}\right] \tag{2}$$

$\mathcal{L}_R$ is a reconstruction loss encouraging the model to encode important information about the trajectories, and $\mathcal{L}_{\text{KL}}$ is a rate regularization, constraining the total amount of information that the model is able to store about the trajectory [Alemi *et al.*, 2017]. For clarity, we use the subscript x_i, to emphasize that these losses are computed as empirical expectations over each of the training trajectories. σ_d^2 are the elements of σ^2 and ϵ is drawn from a normal distribution with mean 0 and diagonal covariance given by σ^2. β is a regularization hyperparameter. Since f returns a full trajectory, we use the subscript t to indicate indexing in to the t^{th} timestep, so it can be compared to the training pose $x_i(t)$.

3.2 TimewarpVAE

A standard approach to learning a manifold for trajectories (see, for example, the method proposed by [Chen and Müller, 2012]) is to map each trajectory to a learned representation that includes information about timing and spatial variations. This type of representation learning can be performed by a beta-VAE [Higgins *et al.*, 2017]. TimewarpVAE is based on beta-VAE, with the goal of separating latent variables for spatial and timing factors to make the models more useful for robot execution. To separate the spatial and temporal variations in trajectories, TimewarpVAE contains two modules not present in beta-VAE: a temporal encoder and a time-warper. The decoder now takes in information from both the spatial encoder and the time-warper. Fig. 4 shows the architecture of TimewarpVAE. It takes in two inputs, the training trajectory x and a desired reconstruction time t. Like in beta-VAE, the spatial encoder maps the trajectory x to its latent value distribution parameterized by z and $\log(\sigma^2)$. The temporal encoder computes time-warping parameters Θ, and the time-warper (defined by the parameters Θ) now acts on t to warp it to a "canonical time" s. The decoder takes the canonical time s and the spatial latent vector and returns the position of the canonical trajectory for that latent vector at the canonical time s. These modules are further explained in Section 4. These functions are jointly trained so the decoded position is a good reconstruction of the position of trajectory x at timestep t, while at the same time minimizing the information that we allow the autoencoder to store about the trajectory.

Specifically, the minimization objective for TimewarpVAE, denoted $\mathcal{L}$, is the sum of the reconstruction cost $\mathcal{L}_R$, beta-VAE's KL divergence loss $\mathcal{L}_{\text{KL}}$, and a new time-warping regularization $\mathcal{L}_\phi$, which we explain further in Section 4.1. $\mathcal{L} = \mathcal{L}_R + \mathcal{L}_{\text{KL}} + \mathcal{L}_\phi$, where

$$\mathcal{L}_R = \frac{1}{\sigma_R^2}\mathbb{E}_{x_i,t,\epsilon}\left[\left\|x_i(t) - f\left(\sum_{j=1}^{k} h(x_i)_j\psi_j(t),\, e(x_i) + \epsilon\right)\right\|^2\right] \tag{3}$$

$$\mathcal{L}_{\text{KL}} = \beta\mathbb{E}_{x_i}\left[\frac{\|e(x_i)\|^2 + \sum_d(\sigma_d^2(x_i) + \log(\sigma_d^2(x_i)))}{2}\right] \tag{4}$$

$$\mathcal{L}_\phi = \lambda\mathbb{E}_{x_i}\left[\frac{1}{K}\sum_{j=1}^{K}(h(x_i)_j - 1)\log(h(x_i)_j)\right] \tag{5}$$

For clarity, we again use the subscript x_i to emphasize that these losses are computed as empirical expectations over each training trajectory x_i. e, σ^2 (and its elements σ_d^2), ϵ, and σ_R^2 are all defined in the same way as for beta-VAE in Eqs. 1 and 2. f is the decoder, now taking in a canonical timestamp along with the latent value. h is the temporal encoder, so that $h(x_i)_j$ is the jth output neuron (out of K total) of the temporal encoder applied to the ith trajectory. The ψ_j are the time-warping basis functions, explained in Sec. 4 and defined in Equation 6. β is a regularization hyperparameter for beta-VAEs. λ is a regularization hyperparameter for our time-warping functions, which we set to 0.05 in our experiments. Since λ penalizes the time-warping in the model, a large $\lambda \to \infty$ would drive time-warping to be the identity function, and $\lambda = 0$ could allow the model to learn severe time-warps. We explain the neural network implementation of all of these functions in the next section.

The benefits of this algorithm are as follows: it learns a low-dimensional representation of spatial variations in trajectories; it can be implemented as a neural network and trained

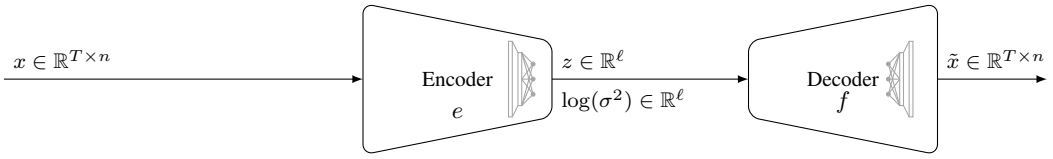

Figure 3: The architecture for Beta-VAE. Beta-VAE takes in a trajectory x, encodes it into a latent distribution parameterized by z and $\log(\sigma^2)$, and decodes to a trajectory $\tilde{x}$.

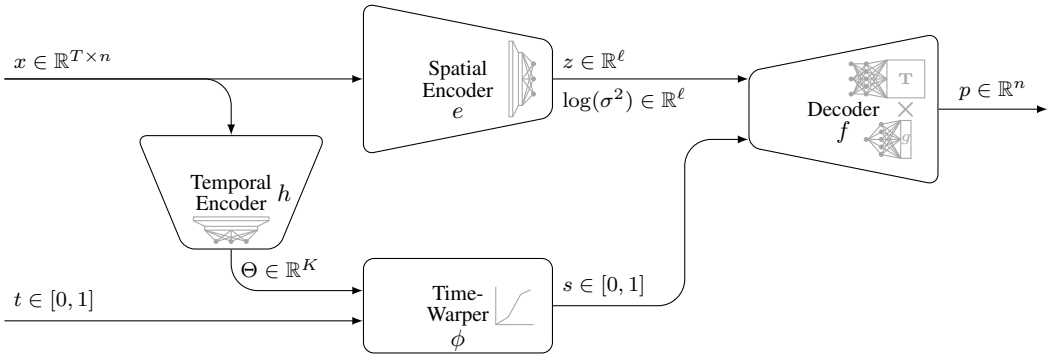

Figure 4: The architecture for TimewarpVAE. TimewarpVAE takes in a full trajectory z and a timestamp t and reconstructs the position p of the trajectory at that timestamp. TimewarpVAE separately encodes the timing of the trajectory into Θ and encodes the spatial information into a latent distribution parameterized by z and $\log(\sigma^2)$.

using backpropagation; and it can accommodate nonlinear timing differences in the training trajectories. Additionally, new trajectories can be generated using a latent value z and canonical timestamps s ranging from 0 to 1 without using the time-warper or the temporal encoder, which we do in our empirical evaluations, calling these generated trajectories "canonical" or "template" trajectories. These trajectories outperform baseline trajectories qualitatively in Fig. 2e and quantitatively in our results section.

4 Neural Network Formulation

This section explains how to write the spatial encoding function, the temporal encoding function, the time-warping function, and the decoding function as differentiable functions. The time-warping function is a differentiable function with no learnable parameters since the time-warping is entirely defined by the input parameters Θ. The other three modules have learnable parameters, which we learn through backprop.

Architecture for the time-warper. The time-warper takes in a training timestamp t for a particular trajectory and maps it monotonically to a canonical timestamp s. ϕ is a piecewise linear function of t with equally spaced knots and K linear segments. The slopes of those segments are labeled by Θ_j for $1 \leq j \leq K$. Different vector $\Theta \in \mathbb{R}^K$ choices give different time-warping functions. In order for Θ to yield a valid time-warping function mapping $[0, 1]$ to $[0, 1]$, the Θ_j should be positive and average to 1. These Θ values are generated by the temporal encoding function discussed in the next paragraph. Given some vector Θ, corresponding to the slope of each segment, the time-warper ϕ is given by $\phi(t) = \sum_{j=1}^{K} \Theta_j \psi_j(t)$ where the ψ_j are defined as follows and do not need to be learned:

$$\psi_j(t) = \min\Big\{ \max\big\{t - (j-1)/K, 0\big\}, 1/K\Big\} \quad (6)$$

A visualization of these basis functions ψ_j is presented in the Appendix. We use the specific parameterization of Θ_j described in the next paragraph to ensure that our time-warping function is a bijection from $[0, 1]$ to $[0, 1]$.

Neural network architecture for the temporal encoder. A neural network $h : \mathbb{R}^{n \times T} \to \mathbb{R}^K$ computes a different vector Θ for each training trajectory x. To ensure the elements of Θ are positive and average to 1, the softmax function is applied to the last layer of the temporal encoder, and the result is scaled by K. This transformation sends the values θ to $\Theta_j = \mathrm{Softmax}(\theta)_j K$ for j from 1 to K, ensuring that the average of the output neurons Θ_j is 1 as desired. By contrast, [Koneripalli *et al.*, 2020] square the last layer and then normalize.

Neural network architecture for the spatial encoder. Given a trajectory x evenly sampled at T different timesteps t_j between 0 and 1, the $T \times n$ matrix of these evenly sampled positions $x(t_j)$ is written as $x \in \mathbb{R}^{n \times T}$. In the neural network architecture used in our experiments, one-dimensional convolutions are applied over the time dimension, treating the n spatial dimensions as input channels. This is followed by different fully connected layers for e and for $\log(\sigma)$. However, any neural network architecture, such as a Transformer [Vaswani *et al.*, 2017] or Recurrent Neural Network [Hochreiter and Schmidhuber, 1997], could be used in the spatial encoder module of a TimewarpVAE.

Neural network architecture for the decoder Any architecture that takes in a time s and a latent vector z and returns

a position p could be used for the decoder f. Our experiments use a modular decomposition of f, with $f(s, z)$ decomposed as the product of a matrix and a vector: $f(s, z) = \mathbf{T}(z)g(s)$. In this formulation, the matrix $\mathbf{T}(z)$ is a function of the latent vector z, and the vector $g(s)$ is a function of the (retimed) timestep s. If each point in the training trajectory has dimension n, and for some hyperparameter m for our architecture, the matrix $\mathbf{T}(z)$ will have shape $n \times m$, and the vector $g(s)$ will be of length m. The nm elements of $\mathbf{T}(z)$ are the (reshaped) output of a sequence of fully connected layers taking the vector z as an input. The m elements of $g(s)$ are computed as the output of a sequence of fully connected layers taking the scalar s as an input. Because the scalar s will lie in the range $[0, 1]$, it is useful to customize the initialization of the weights in the first hidden layer of $g(s)$. Details of the custom initialization are provided in the Appendix. This chosen architecture is useful for easily creating the "NoNonlinearity" ablation experiment in Section 5.5. With this architecture, if the hidden layers in $\mathbf{T}(z)$ are removed, then it a linear function of z, and so then entire decoder becomes linear with respect to z, so the generated position p will be a linear combination of possible positions at timestep s.

4.1 Regularization of Time-Warping Function

The choice of timing for the canonical trajectories adds a degeneracy to the solution.[2] Without our regularization, it is possible for other methods, like Rate Invariant AE, to warp so severely that they can ignore parts of the canonical trajectory. This is a problem if we generate robot motions from the canonical trajectory since it can lead to jittering motions, as seen at the beginning and end of the trajectory in Fig. 2d.

We propose a regularization penalty on the time-warper ϕ to choose among the degenerate solutions. The proposed penalty is on $\int_0^1 (\phi'(t) - 1) \log(\phi'(t))\ dt$. That regularization contains the function $g(x) = (x-1)\log(x)$ applied to the slope $\phi'(t)$, integrated over each point t. That function $g(x)$ is concave-up for $x > 0$ and takes on a minimum at $x = 1$, encouraging the slope of ϕ to be near 1. This formulation has the symmetric property that regularizing $\phi(t)$ gives the exact same regularization as regularizing $\phi^{-1}(s)$. This symmetry is proven in the Appendix. For each trajectory x_i our time-warper ϕ is stepwise linear with K equally-sized segments with slopes $\Theta_1 = h(x_i)_1, \ldots, \Theta_k = h(x_i)_K$. Thus, the regularization integral for the time-warper associated with x_i is

$$\mathcal{L}_\phi(x_i) = \frac{1}{K} \sum_{j=1}^{K} (h(x_i)_j - 1) \log(h(x_i)_j) \tag{7}$$

5 Experiments

Experiments are performed on two datasets, one containing handwriting gestures made in the air while holding a Wii remote [Chen *et al.*, 2012], and one that we collect ourselves, containing motions that pick up yarn off a plate with a fork, mimicking food acquisition. The same model architecture is used for both experiments, with hyperparameters given in the Appendix. Additionally, during training, we perform data augmentation by randomly perturbing the timesteps used when sampling the trajectory x, using linear interpolation to compute sampled positions. Our specific data-augmentation implementation is described in the Appendix. This data augmentation decreases training performance but greatly improves test performance, as shown in the ablation studies.

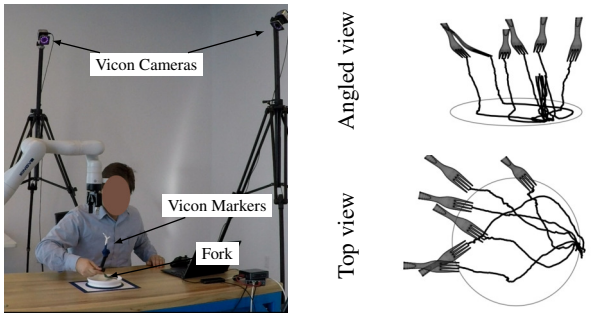

(a) The demonstration system (b) Six demonstrations[3]

Figure 5: We collect trajectory recordings of the position and orientation of a fork while it is used to pick a small piece of yarn off a plate with steep sides. Example trajectories are presented from two angles, showing the initial orientation of the fork and the position of the tip of the fork over time.

5.1 Fork Trajectory Dataset

345 fork trajectories are recorded using the Vicon tracking system shown in Fig. 5a. Reflective markers are rigidly attached to a plastic fork, and the trajectory of the fork is recorded using Vicon cameras. A six-centimeter length of yarn is placed on the plate in an arbitrary location and orientation. It is then picked up right-handed by scraping it to the left and using the side of the plate as a static tool to push it onto the fork. Demonstrations were intentionally collected with three different timings, where in some trajectories the approach to the plate was intentionally much faster than the retreat from the plate, in some trajectories the approach was intentionally much slower than the retreat from the plate, and in the remaining trajectories the approach and retreat are approximately the same speed. The dataset was split into 240 training trajectories and 105 test trajectories. Examples of six recorded trajectories, along with visualizations of the starting pose of the fork for those trajectories, are presented in Fig. 5b. Trajectories are truncated to start when the fork tip passes within 10cm of the table and to end again when the fork passes above 10cm. All trajectories were subsampled to 200 equally-spaced time points, using linear interpolation as needed. We express the data as the x, y, z position of the tip of the fork and the rw, rx, ry, rz quaternion orientation of the fork, giving a dataset of dimension $n = 7$ at each data-

[2] This is similar to the degeneracy noted in the Appendix for continuous dynamic time warping [Kruskal and Liberman, 1983], and, as noted in the Appendix, was not properly analyzed in [Shapira Weber *et al.*, 2019].

[3] Fork meshes in 3D trajectory plots were downloaded and modified from https://www.turbosquid.com/3d-models/metal-fork-3d-model/362158 and are used under the TurboSquid 3D Model License

Architecture	Beta	Rate	Training A-RMSE ($\pm 3\sigma$)	Test A-RMSE ($\pm 3\sigma$)
TimewarpVAE	0.01	3.716	0.187 ± 0.003	$\mathbf{0.233 \pm 0.003}$
	0.1	3.227	$\mathbf{0.185 \pm 0.007}$	0.234 ± 0.008
RateInvariantAE	0.01	4.095	0.260 ± 0.130	0.316 ± 0.188
	0.1	3.280	0.285 ± 0.154	0.325 ± 0.132
beta-VAE	0.01	4.759	0.291 ± 0.005	0.343 ± 0.016
	0.1	3.670	0.293 ± 0.007	0.342 ± 0.011
NoTimewarp	0.01	3.924	0.264 ± 0.007	0.360 ± 0.017
	0.1	3.508	0.265 ± 0.006	0.354 ± 0.014

Table 1: Performance results for 3-dimensional models of fork trajectories. Our TimewarpVAE significantly outperforms beta-VAE and the ablation of TimewarpVAE without the time-warper.

point. The data is preprocessed to choose a consistent sign of the quaternion representations so they are all near each other in $\mathbb{R}^4$. The data is mean-centered by subtracting the average x, y, z, rw, rx, ry, rz training values, and the x, y, z values are divided by a normalizing factor so that their combined variance $\mathbb{E}[x^2 + y^2 + z^2]$ is 3 on the training set. Likewise, the rw, rx, ry, rz values are multiplied by a scaling factor of $0.08m$, (chosen as a length scale associated with the size of the fork), before dividing by the same normalizing factor, to bring all the dimensions into the same range.

5.2 Handwriting Gestures Dataset

The air-handwriting dataset collected by [Chen *et al.*, 2012] is used for the handwriting experiment. The drawn letters are projected onto xy coordinates. A training set of 125 random examples of the letter "A" are drawn from the air-handwriting dataset , and the remaining 125 random examples of the letter "A" are the test set. All trajectories were subsampled to 200 equally-spaced time points, using linear interpolation as needed. The data are mean-centered so that the average position over the whole training dataset is the origin, and x and y are scaled together by the same constant so that their combined variance $\mathbb{E}[x^2 + y^2]$ is 2 on the training set. Example training trajectories are in the Appendix.

5.3 Model Performance Measures

The performance measures include three important values: the training reconstruction error, the test reconstruction error, and the model rate. To measure spatial variation of trajectories, reconstruction errors are computed by first performing symmetric DTW to align the reconstructed trajectory to the original trajectory. We then compute the Euclidean mean squared error between each point in the original trajectory and every point it is paired with. After that, we calculate the average of all those errors over all the timesteps in the original trajectory before taking the square root to compute our aligned root mean squared error (A-RMSE). In the framework of Rate-Distortion theory, these errors are distortion terms. The model rate measures the information bottleneck imposed by the model and is given by the KL divergence term in the beta-VAE loss function. It's important to check the rate of the model since arbitrarily complex models can get perfect reconstruction error if they have a large enough rate [Alemi *et al.*, 2018]. However, among trained models with similar rates, it is fair to say that the model with lower distortion is a better model. Model rate is reported in bits.

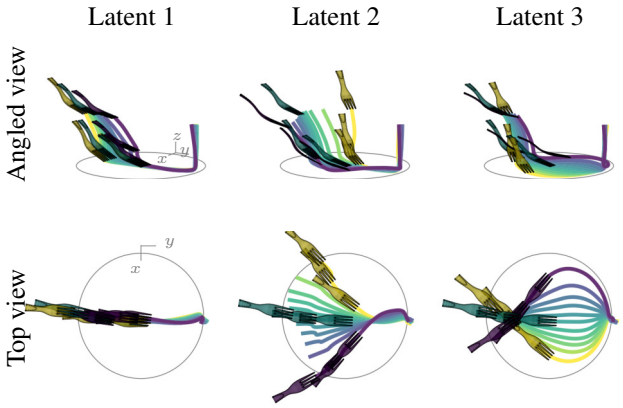

Figure 6: The paths of the fork tip are plotted over time for TimewarpVAE trajectories using different latent vectors. The orientation of the fork is shown at three different timesteps in a color matching the associated path. Each latent dimension has an interpretable effect. The first latent determines the fork's initial y position, the second latent determines the fork's initial x position, and the third latent determines how the fork curves during trajectory execution.

5.4 Fork Model Results

Models are trained with a latent dimension of three on the fork dataset. TimewarpVAE is compared to beta-VAE, a VAE version of Rate Invariant AE, and an ablation of TimewarpVAE called "NoTimewarp" that sets the timewarping module to the identity function. The latent sweep of a TimewarpVAE trained with $\beta = 1$ is shown in Fig. 6, showing its interpretable latent space. Table 1 shows performance measures, where we compute and summarize five trials for each model type for various hyperparameters β. TimewarpVAE outperforms the baseline methods.

5.5 Air Handwriting Results

TimewarpVAE is compared to baseline methods trained on the same training and test splits. All models are trained with a batch size of 64 for 20,000 epochs, using the Adam optimizer and a learning rate 0.001. We train each model five times for different choices of beta, and we plot the mean and one standard error above and below the mean. To give context to these results, we also show results for parametric dynamic movement primitives (Parametric DMPs) [Matsubara *et al.*, 2011] and PCA results, which do not have associated rate values. TimewarpVAE significantly outperforms Parametric DMPs, PCA, and beta-VAE, with the greatest differences for smaller latent dimensions. TimewarpVAE shows comparable performance to RateInvariant on training error and consistently outperforms RateInvariant in test error.

Ablation studies were run to understand the importance of different architecture choices. The first removes the data augmentation of additional trajectories with perturbed timings. We call this ablation"NoAugment." The second removes the hidden layers in the neural network $\mathbf{T}(z)$. Removing the hidden layers makes $\mathbf{T}(z)$ a linear function, meaning the func-

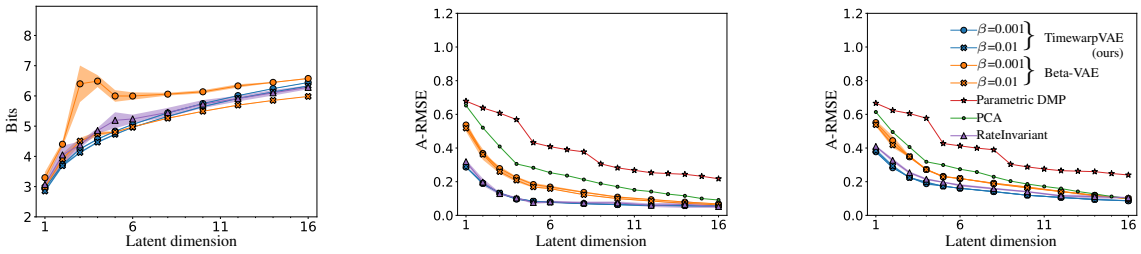

(a) Rate (b) Train Distortion (c) Test Distortion

Figure 7: TimewarpVAE compared to beta-VAE, Parametric DMP, PCA, and Rate Invariant AE. Especially for lower-dimensional models, TimewarpVAE performs comparably to RateInvariant on training error and consistently outperforms RateInvariant in test error.

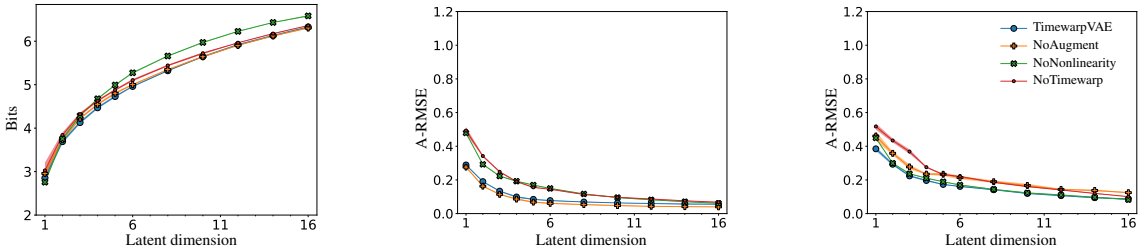

(a) Rate (b) Train Distortion (c) Test Distortion

Figure 8: Ablation results show the data augmentation of timing noise is important for generalization performance, the nonlinear model gives a better fit to training data without losing generalization performance, and the time-warper is key to TimewarpVAE's good performance.

tion f can only learn trajectories that are a linear function of the latent variable z (but f is still nonlinear in the time argument s). We call this ablation "NoNonlinearity". The third removes the time-warper and replaces it with the identity function. We call this ablation "NoTimewarp." Results for these ablations are plotted in Fig. 8. NoAugment confirms the importance of data augmentation for good generalization. NoAugment can get a slightly better fit to the training data than TimewarpVAE, but performs poorly on test data. NoNonlinearity has comparable performance on the test data to TimewarpVAE, showing the strict regularization imposed by its linearity condition is good for generalization. However, NoNonlineary has such strong regularization that it cannot fit the training data as closely. Additionally, the model rate for NoNonlinearity is higher. By constraining our model to be linear in the latent term, we cannot compress information as efficiently into the latent space. Without the ability to time-align the data, NoTimewarping is not able to fit either the training or test data well. The information rate of NoTimewarping is the same as that of TimewarpVAE, showing it does not compress spatial information as efficiently.

Robot Execution. We demonstrate the usefulness of our algorithm on a Kinova Gen3 robot arm. Because of our timing regularization term, we can optimize various timing options during the replay of the trajectory, constraining the trajectory to stay close to the demonstrated timings. This timing optimization allows the robot to consider its joint torque and speed limitations and choose a timing that it can execute the quickest under those constraints. An example is shown in Fig. 1. If the robot can only scale the timing uniformly, the optimized trajectory takes 1.8 times longer to execute. Our approach gives the robot the flexibility to slow down some parts of the trajectory and speed up other parts.

6 Discussion

TimewarpVAE is useful for simultaneously learning timing variations and latent factors of spatial variations. Because it separately models timing variations, TimewarpVAE concentrates the modeling capacity of its spatial latent variable on spatial factors of variation. As discussed further in the Appendix, TimewarpVAE can be viewed as a natural extension of continuous DTW. TimewarpVAE uses a parametric model for the time-warping function. A different approach could be to use a non-parametric model like DTW to warp the reconstructed trajectory to the input trajectory and then backpropagate the aligned error. That alternate approach has a much higher computation cost because it requires computing DTW for each trajectory at each learning step and does not re-use the time-warper from previous steps. We consider this approach briefly in the Appendix and leave it to future work to more fully understand the benefits of this alternate implementation and when it should be used or combined with the proposed TimewarpVAE. This work measured the spatial error of reconstructed training and test trajectories, and showed the TrajectoryVAE does a better job than beta-VAE at compressing spatial information into small latent spaces. Future work will investigate also compressing the latent timing information.

Acknowledgments
The authors would like to thank Sloan Nietert, Ziv Goldfeld, and Tapomayukh Bhattacharjee for valuable conversations and insights.

Reproducibility statement
Our experiments are performed on a publicly available human gesture dataset of air-handwriting [Chen *et al.*, 2012], and on a dataset of quasistatic manipulation which we make publically available at https://github.com/travers-rhodes/TimewarpVAE. The PyTorch implementation of TimewarpVAE used in our experiments is also included at that url, as well as the code to generate the figures for this paper.

References

[Alemi *et al.*, 2017] Alexander A. Alemi, Ian Fischer, Joshua V. Dillon, and Kevin Murphy. Deep variational information bottleneck. In *5th International Conference on Learning Representations, ICLR 2017, Toulon, France, April 24-26, 2017, Conference Track Proceedings*. OpenReview.net, 2017.

[Alemi *et al.*, 2018] Alexander Alemi, Ben Poole, Ian Fischer, Joshua Dillon, Rif A. Saurous, and Kevin Murphy. Fixing a Broken ELBO. In *Proceedings of the 35th International Conference on Machine Learning*, pages 159–168. PMLR, July 2018. ISSN: 2640-3498.

[Chang *et al.*, 2021] Xiaobin Chang, Frederick Tung, and Greg Mori. Learning discriminative prototypes with dynamic time warping. In *2021 IEEE/CVF Conference on Computer Vision and Pattern Recognition (CVPR)*. IEEE, June 2021.

[Chen and Müller, 2012] Dong Chen and Hans-Georg Müller. Nonlinear manifold representations for functional data. *The Annals of Statistics*, 40(1), February 2012.

[Chen *et al.*, 2012] Mingyu Chen, Ghassan AlRegib, and Biing-Hwang Juang. 6DMG: a new 6D motion gesture database. In *Proceedings of the 3rd Multimedia Systems Conference*, MMSys '12, pages 83–88, New York, NY, USA, February 2012. Association for Computing Machinery.

[Chen *et al.*, 2016] Nutan Chen, Maximilian Karl, and Patrick van der Smagt. Dynamic movement primitives in latent space of time-dependent variational autoencoders. In *2016 IEEE-RAS 16th International Conference on Humanoid Robots (Humanoids)*. IEEE, November 2016.

[Chen *et al.*, 2021] Xinyu Chen, Jiajie Xu, Rui Zhou, Wei Chen, Junhua Fang, and Chengfei Liu. Trajvae: A variational autoencoder model for trajectory generation. *Neurocomputing*, 428:332–339, March 2021.

[Cho *et al.*, 2023] Cheol Jun Cho, Edward Chang, and Gopala Anumanchipalli. Neural latent aligner: Cross-trial alignment for learning representations of complex, naturalistic neural data. In Andreas Krause, Emma Brunskill, Kyunghyun Cho, Barbara Engelhardt, Sivan Sabato, and Jonathan Scarlett, editors, *Proceedings of the 40th International Conference on Machine Learning*, volume 202 of *Proceedings of Machine Learning Research*, pages 5661–5676. PMLR, 23–29 Jul 2023.

[Clevert *et al.*, 2016] Djork-Arné Clevert, Thomas Unterthiner, and Sepp Hochreiter. Fast and accurate deep network learning by exponential linear units (elus). In Yoshua Bengio and Yann LeCun, editors, *4th International Conference on Learning Representations, ICLR 2016, San Juan, Puerto Rico, May 2-4, 2016, Conference Track Proceedings*, 2016.

[Coll-Vinent and Vondrick, 2022] Didac Suris Coll-Vinent and Carl Vondrick. Representing spatial trajectories as distributions. In Alice H. Oh, Alekh Agarwal, Danielle Belgrave, and Kyunghyun Cho, editors, *Advances in Neural Information Processing Systems*, 2022.

[Cuturi and Blondel, 2017] Marco Cuturi and Mathieu Blondel. Soft-DTW: a differentiable loss function for time-series. In Doina Precup and Yee Whye Teh, editors, *Proceedings of the 34th International Conference on Machine Learning*, volume 70 of *Proceedings of Machine Learning Research*, pages 894–903. PMLR, 06–11 Aug 2017.

[Fréchet, 1906] M. Maurice Fréchet. Sur quelques points du calcul fonctionnel. *Rendiconti del Circolo Matematico di Palermo*, 22(1):1–72, December 1906.

[Giorgino, 2009] Toni Giorgino. Computing and visualizing dynamic time warping alignments in r: The dtw package. *Journal of Statistical Software*, 31(7), 2009.

[Graves *et al.*, 2006] Alex Graves, Santiago Fernández, Faustino Gomez, and Jürgen Schmidhuber. Connectionist temporal classification. In *Proceedings of the 23rd international conference on Machine learning - ICML '06*. ACM Press, 2006.

[Hargraves and Paris, 1987] C.R. Hargraves and S.W. Paris. Direct trajectory optimization using nonlinear programming and collocation. *Journal of Guidance, Control, and Dynamics*, 10(4):338–342, July 1987.

[Higgins *et al.*, 2017] Irina Higgins, Loïc Matthey, Arka Pal, Christopher P. Burgess, Xavier Glorot, Matthew M. Botvinick, Shakir Mohamed, and Alexander Lerchner. beta-vae: Learning basic visual concepts with a constrained variational framework. In *5th International Conference on Learning Representations, ICLR 2017, Toulon, France, April 24-26, 2017, Conference Track Proceedings*. OpenReview.net, 2017.

[Hochreiter and Schmidhuber, 1997] Sepp Hochreiter and Jürgen Schmidhuber. Long short-term memory. *Neural computation*, 9(8):1735–1780, 1997.

[Ijspeert *et al.*, 2013] Auke Jan Ijspeert, Jun Nakanishi, Heiko Hoffmann, Peter Pastor, and Stefan Schaal. Dynamical movement primitives: Learning attractor models for motor behaviors. *Neural Computation*, 25(2):328–373, February 2013.

[Kneip and Ramsay, 2008] Alois Kneip and James O Ramsay. Combining registration and fitting for functional models. *Journal of the American Statistical Association*, 103(483):1155–1165, September 2008.

[Koneripalli *et al.*, 2020] Kaushik Koneripalli, Suhas Lohit, Rushil Anirudh, and Pavan Turaga. Rate-invariant autoencoding of time-series. In *ICASSP 2020 - 2020 IEEE International Conference on Acoustics, Speech and Signal Processing (ICASSP)*. IEEE, May 2020.

[Kruskal and Liberman, 1983] Joseph B. Kruskal and Mark Liberman. The symmetric time-warping problem: From continuous to discrete. In David Sankoff and Joseph B. Kruskal, editors, *Time Warps, String Edits, and Macromolecules : The Theory and Practice of Sequence Comparison*, chapter 4. Addison-Wesley Pub. Co., Advanced Book Program, Reading, Mass., 1983.

[Kuester *et al.*, 2021] J. Kuester, W. Gross, and W. Middelmann. 1d-convolutional autoencoder based hyperspectral data compression. *The International Archives of the Photogrammetry, Remote Sensing and Spatial Information Sciences*, XLIII-B1-2021:15–21, 2021.

[Kumar and Poole, 2020] Abhishek Kumar and Ben Poole. On implicit regularization in β-vaes. In *International Conference on Machine Learning*, pages 5480–5490. PMLR, 2020.

[Lu *et al.*, 2019] Xiaoyu Lu, Jan Stuehmer, and Katja Hofmann. Trajectory VAE for multi-modal imitation, 2019.

[Matsubara *et al.*, 2011] Takamitsu Matsubara, Sang-Ho Hyon, and Jun Morimoto. Learning parametric dynamic movement primitives from multiple demonstrations. *Neural Networks*, 24(5):493–500, June 2011.

[Petitjean *et al.*, 2011] François Petitjean, Alain Ketterlin, and Pierre Gançarski. A global averaging method for dynamic time warping, with applications to clustering. *Pattern Recognition*, 44(3):678–693, March 2011.

[Sakoe and Chiba, 1978] H. Sakoe and S. Chiba. Dynamic programming algorithm optimization for spoken word recognition. *IEEE Transactions on Acoustics, Speech, and Signal Processing*, 26(1):43–49, February 1978. Conference Name: IEEE Transactions on Acoustics, Speech, and Signal Processing.

[Schaal *et al.*, 2007] Stefan Schaal, Peyman Mohajerian, and Auke Ijspeert. Dynamics systems vs. optimal control — a unifying view. In *Progress in Brain Research*, pages 425–445. Elsevier, 2007.

[Schultz and Jain, 2018] David Schultz and Brijnesh Jain. Nonsmooth analysis and subgradient methods for averaging in dynamic time warping spaces. *Pattern Recognition*, 74:340–358, February 2018.

[Shapira Weber *et al.*, 2019] Ron A Shapira Weber, Matan Eyal, Nicki Skafte, Oren Shriki, and Oren Freifeld. Diffeomorphic temporal alignment nets. In H. Wallach, H. Larochelle, A. Beygelzimer, F. d'Alché-Buc, E. Fox, and R. Garnett, editors, *Advances in Neural Information Processing Systems*, volume 32. Curran Associates, Inc., 2019.

[Tedrake and the Drake Development Team, 2019] Russ Tedrake and the Drake Development Team. Drake: Model-based design and verification for robotics, 2019.

[Trigeorgis *et al.*, 2018] George Trigeorgis, Mihalis A. Nicolaou, Bjorn W. Schuller, and Stefanos Zafeiriou. Deep canonical time warping for simultaneous alignment and representation learning of sequences. *IEEE Transactions on Pattern Analysis and Machine Intelligence*, 40(5):1128–1138, May 2018.

[Vaswani *et al.*, 2017] Ashish Vaswani, Noam Shazeer, Niki Parmar, Jakob Uszkoreit, Llion Jones, Aidan N Gomez, Ł ukasz Kaiser, and Illia Polosukhin. Attention is all you need. In I. Guyon, U. Von Luxburg, S. Bengio, H. Wallach, R. Fergus, S. Vishwanathan, and R. Garnett, editors, *Advances in Neural Information Processing Systems*, volume 30. Curran Associates, Inc., 2017.

[Wächter and Biegler, 2005] Andreas Wächter and Lorenz T. Biegler. On the implementation of an interior-point filter line-search algorithm for large-scale nonlinear programming. *Mathematical Programming*, 106(1):25–57, April 2005.

[Wang *et al.*, 2016] Jane-Ling Wang, Jeng-Min Chiou, and Hans-Georg Müller. Functional data analysis. *Annual Review of Statistics and Its Application*, 3(1):257–295, June 2016.

[Williams *et al.*, 2020] Alex H. Williams, Ben Poole, Niru Maheswaranathan, Ashesh K. Dhawale, Tucker Fisher, Christopher D. Wilson, David H. Brann, Eric M. Trautmann, Stephen Ryu, Roman Shusterman, Dmitry Rinberg, Bence P. Ölveczky, Krishna V. Shenoy, and Surya Ganguli. Discovering precise temporal patterns in large-scale neural recordings through robust and interpretable time warping. *Neuron*, 105(2):246–259.e8, January 2020.

[Zhou and la Torre, 2012] Feng Zhou and F. De la Torre. Generalized time warping for multi-modal alignment of human motion. In *2012 IEEE Conference on Computer Vision and Pattern Recognition*. IEEE, June 2012.

A Supplemental Materials

A.1 Derivation of TimewarpVAE from Dynamic Time Warping

Dynamic time warping (DTW) compensates for timing differences between two trajectories by retiming the two trajectories so that they are spatially close to each other at matching timestamps. In this section, we explicitly derive TimewarpVAE from continuous dynamic time warping, the formulation of dynamic time warping for continuous functions presented by [Kruskal and Liberman, 1983].

Continuous Dynamic Time Warping

We begin with a brief summary of continuous DTW. Given two trajectories x_0 and x_1 (each a function from time in $[0, 1]$ to some position in $\mathbb{R}^n$), continuous DTW learns two time-warping functions, ρ_0 and ρ_1, where each time-warping function is monotonic and bijective from $[0, 1]$ to $[0, 1]$. The goal is to have the time-warped trajectories be near each other at corresponding (warped) timesteps. Mathematically, ρ_0 and ρ_1 are chosen to minimize the integral

$$\int_0^1 \left\| x_1\left(\rho_1(s)\right) - x_0\left(\rho_0(s)\right)\right\|^2 \frac{(\rho_0)'(s) + (\rho_1)'(s)}{2}\, ds \tag{8}$$

This integral is the distance between the trajectories at corresponding timesteps, integrated over a symmetric weighting factor.

This algorithm has a degeneracy, in that many different ρ_0 and ρ_1 will lead to equivalent alignments $\rho_1 \circ \rho_0^{-1}$ and will therefore have equal values of our cost function. This becomes relevant when generating new trajectories from the interpolated model, as it requires choosing a timing for the generated trajectory.

Reformulation of Continuous DTW

The optimization criterion of continuous DTW can be rewritten as follows: Given the time-warping functions ρ_0 and ρ_1 from above, define $\phi_0 = \rho_0^{-1}$ and $\phi_1 = \rho_1^{-1}$. Let the function $f : [0, 1] \times [0, 1] \to \mathbb{R}^n$ be defined as $f(s, z) = (1 - z)x_0(\rho_0(s)) + zx_1(\rho_1(t))$. That is, $f(s, z)$ is the unique function that is linear in its second parameter and which satisfies the boundary conditions $f(\phi_0(t), 0) = x_0(t)$ and $f(\phi_1(t), 1) = x_1(t)$. These boundary conditions associate x_0 with $z_0 = 0$ and x_1 with $z_1 = 1$.

Our minimization objective for choosing ρ_0 and ρ_1 (or, equivalently, for choosing their inverses ϕ_0 and ϕ_1) can be written in terms of f as

$$\frac{1}{2}\int_0^1 \left\| \frac{\partial f(s,z)}{\partial z}\Big|_{s=\phi_0(t),z=0} \right\|^2 dt + \frac{1}{2}\int_0^1 \left\| \frac{\partial f(s,z)}{\partial z}\Big|_{s=\phi_1(t),z=1} \right\|^2 dt. \tag{9}$$

The derivation goes as follows: We define $\phi_0 = \rho^{-1}$ and $\phi_1 = \rho^{-1}$, and we define the function $f : [0, 1] \times [0, 1] \to \mathbb{R}^n$ to be the unique function that is linear in its second parameter and which satisfies the boundary conditions $f(\phi_0(t), 0) = x_0(t)$ and $f(\phi_1(t), 1) = x_1(t)$. Equivalently, it satisfies the boundary conditions $f(s, 0) = x_0(\phi_0^{-1}(s))$ and $f(s, 1) = x_1(\phi_1^{-1}(s))$.

Substituting these definitions gives an optimization criterion of

$$\int_0^1 \left\| x_1\left(\phi_1^{-1}(s)\right) - x_0\left(\phi_0^{-1}(s)\right)\right\|^2 \frac{\left(\phi_0^{-1}\right)'(s) + \left(\phi_1^{-1}\right)'(s)}{2}\, ds \tag{10}$$

The boundary conditions of f imply this is equal to

$$\frac{1}{2}\int_0^1 \|f(s, 1) - f(s, 0)\|\, d\phi_0^{-1}(s) + \frac{1}{2}\int_0^1 \|f(s, 1) - f(s, 0)\|\, d\phi_1^{-1}(s) \tag{11}$$

And now, performing a change-of-variables $u = \phi_0^{-1}(s)$ and $v = \phi_1^{-1}(s)$ gives

$$\frac{1}{2}\int_0^1 \|f(\phi_0(u), 1) - f(\phi_0(u), 0)\|^2\, du + \frac{1}{2}\int_0^1 \|f(\phi_1(v), 1) - f(\phi_1(v), 0)\|^2\, dv \tag{12}$$

Since f is linear in its second coordinate, we can write this in terms of the partial derivatives of f

$$\frac{1}{2}\int_0^1 \left\| \frac{\partial f(s,z)}{\partial z}\Big|_{s=\phi_0(u),z=0} \right\|^2 du + \frac{1}{2}\int_0^1 \left\| \frac{\partial f(s,z)}{\partial z}\Big|_{s=\phi_1(v),z=1} \right\|^2 dv \tag{13}$$

Simultaneous Time-Warping and Manifold Learning on Trajectories

The relation to TimewarpVAE is as follows:

For each trajectory x_i, TimewarpVAE learns a low-dimensional latent representation $z_i \in \mathbb{R}^\ell$ associated with that trajectory. These z_i are the natural generalizations of the reformulation of continuous DTW above, which had hard-coded latent values $z_0 = 0$ and $z_1 = 1$ for the two trajectories.

For each trajectory x_i, TimewarpVAE learns a time-warping function ϕ_i that transforms timesteps to new canonical timings. These ϕ_i are the natural extension of the ϕ_0 and ϕ_1 from above.

TimewarpVAE learns a generative function f which, given a canonical timestamp s and a latent value z, returns the positon corresponding to the trajectory at that time. This is an extension of the function f, with relaxations on the linearity constraint and the boundary conditions. Instead of requiring f to be linear in the z argument, we parameterize f with a neural network and regularize it to encourage f to have small partial derivative with respect to the latent variable z. This regularization is described in Section A.1. Instead of a boundary constraints requiring $f(\phi_i(t), z_i)$ to be equal to $x_i(t)$, we instead add an optimization objective that $f(\phi_i(t), z_i)$ be close to $x_i(t)$,

Regularization of the Decoder

Training the decoder using our optimization objective includes adding noise ϵ to the latent values z before decoding. This encourages the decoder to take on similar values for nearby values of z. In particular, as described by [Kumar and Poole, 2020], this will add an implicit Jacobian squared regularization of the decoder over the z directions. Penalizing these $\|\frac{\partial f(s,z)}{\partial z}\|^2$ terms is exactly what we want for our manifold-learning algorithm. Additionally, we note that we do not add any noise to the temporal encoder when computing the reconstruction loss, so our beta-VAE style architecture does not include any unwanted regularization of $\|\frac{\partial f(s,z)}{\partial s}\|^2$.

A.2 Degeneracy of Time Warping Using Notation of [Shapira Weber *et al.*, 2019]

Using the notation of [Shapira Weber *et al.*, 2019], the timing degeneracy noted in the main paper also applies. For any set of time-warping functions T^{θ_i}, one for each of the N_k different trajectories u_i with class label y_i out of K possible class labels, all of those time-warping functions can be composed with some additional fixed diffeomorphic warping T^p without changing the Inverse Consistency Averaging Error.

That is, composing all time-warps with a time-warping function T^p to generate $\tilde{T}^{\theta_i} = T^{\theta_i} \circ T^p$ will not affect the Inverse Consistency Averaging Error, since now the (perturbed) average warped trajectory for cluster k $\tilde{\mu}_k$ is the warp of the previous average warped trajectory μ_k

$$\tilde{\mu}_k = \frac{1}{N_k} \sum u_i \circ T^{\theta_i} \circ T^p = \frac{1}{N_k} \left(\sum u_i \circ T^{\theta_i} \right) \circ T^p = \mu \circ T^p \tag{14}$$

.

The inverse $\tilde{T}^{-\theta_i}$ is simply $T^{-p} \circ T^{-\theta_i}$

The Inverse Consistency Averaging Error using those perturbed time-warps $\tilde{T}$ is the same as that computed using the original time-warps.

$$\mathcal{L}_{ICAE}(\tilde{T}) = \sum_{k=1}^{K} \frac{1}{N_K} \sum_{i:y_i=k} \left\| \tilde{\mu}_k \circ \tilde{T}^{\theta_i} - u_i \right\|_{\ell_2}^2 \tag{15}$$

$$= \sum_{k=1}^{K} \frac{1}{N_K} \sum_{i:y_i=k} \left\| \mu_k \circ T^p \circ T^{-p} \circ T^{-\theta_i} - u_i \right\|_{\ell_2}^2 \tag{16}$$

$$= \sum_{k=1}^{K} \frac{1}{N_K} \sum_{i:y_i=k} \left\| \mu_k \circ T^{-\theta_i} - u_i \right\|_{\ell_2}^2 \tag{17}$$

$$= \mathcal{L}_{ICAE}(T) \tag{18}$$

This shows that there is a degeneracy over the choice of warping of the warped trajectories. Warped trajectories can all be additionally warped by another time-warping function without changing the Inverse Consistency Averaging Error.

A.3 Plot of time-warping basis function

A plot of the time-warping basis functions ψ is shown in Fig. 9.

A.4 Example training trajectories of letter "A"

Example training trajectories of handwritten letter "A"'s are shown in Fig. 10.

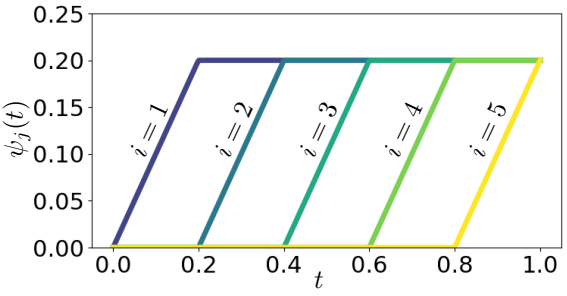

Figure 9: Time alignment basis functions for $K = 5$, for each i from 1 to 5

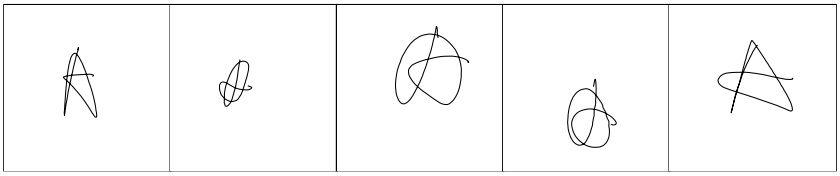

Figure 10: Five example trajectories of handwritten "A"

A.5 Time-Warper Effect on Trained Model

In Fig. 11 we show how varying the time-warper parameters affects the timing of the generated trajectory for one of the TimewarpVAE letter models. Here, we choose five different sets of time-warper parameters, and plot the resulting time-warper function $\phi(t)$. We then decode the same spatial trajectory using those five latent parameters. The resulting trajectories spatially would look all the same, and we plot the X and Y locations of the generated trajectories as a function of time. The associated timings of the trajectories changes due to the time-warper function.

A.6 Additional Interpolations for Models

Here, we present additional interpolation results, all on 16 latent dimensions and $\beta = 0.001$. We note that the convolutional encoder/decoder architecture in beta-VAE in Fig. 12b does not appear to have as strong an implicit bias toward smooth trajectories as the TimewarpVAE architecture. This makes sense because the TimewarpVAE architecture decomposes the generative function into a component $g(s)$ which computes poses as a function of time, likely inducing an inductive bias toward smoother trajectories as a function of time.

The interpolation in Fig. 12a shows that in the ablation of TimewarpVAE without the timing module the interpolation does not preserve the style of the "A". Likewise, the DMP interpolation in Fig. 12c does not preserve the style of the "A".

A.7 Equivalence of Regularizing ϕ or ϕ^{-1}

We note that our regularization is the same, regardless if we regularize ϕ or ϕ^{-1}. We show this by applying the substitution $s = \phi(t)$, $ds = \phi'(t)dt$. That substitution gives: $\int_0^1 \left(1 - \frac{1}{\phi'(\phi^{-1}(s))}\right) \log\left(\phi'(\phi^{-1}(s))\right) ds$.

We use the identity $(\phi^{-1})'(s) = \frac{1}{\phi'(\phi^{-1}(s))}$ to simplify to

$$\int_0^1 \left(1 - (\phi^{-1})'(s)\right) \log\left(\frac{1}{(\phi^{-1})'(s)}\right) ds = \int_0^1 \left((\phi^{-1})'(s) - 1\right) \log\left((\phi^{-1})'(s)\right) ds \tag{19}$$

This is exactly our regularization applied to the function ϕ^{-1}. Thus, we note that our regularization is symmetric. Our regularization cost is the same whether it is applied to ϕ (the function from trajectory time to canonical time) or applied to ϕ^{-1} (the function from canonical time to trajectory time).

It didn't have to be that way. For example, if our cost function were of the form $\int_0^1 \log^2(\phi'(t))dt$, the substitution above would give a cost $\int_0^1 \frac{1}{\phi'(\phi^{-1}(s))} \log^2(\phi'(\phi^{-1}(s)))ds$ which simplifies to $\int_0^1 \frac{1}{\phi'(\phi^{-1}(s))} \log^2((\phi^{-1})'(s))ds$ which equals $\int_0^1 (\phi^{-1})'(s) \log^2((\phi^{-1})'(s))ds$ which is different from applying the regularization procedure to ϕ^{-1} which would have given a regularization term of: $\int_0^1 \log^2((\phi^{-1})'(s))ds$

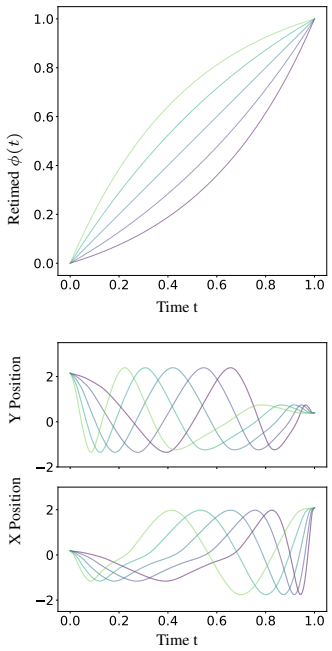

Figure 11: Decoding the same spatial latent variable using different time-warping parameters will give the same spatial trajectory but with different timings (fast or slow at different times). We plot the time-warping functions for five different timing latents and the generated trajectories for a single spatial latent value by showing the generated positions as a function of time.

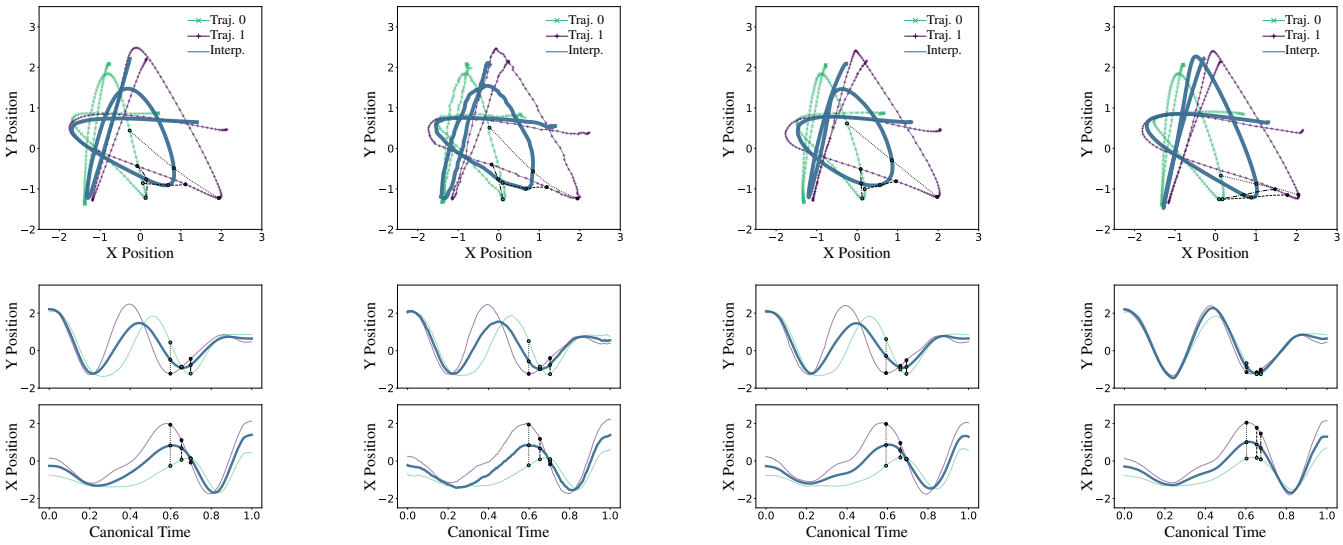

(a) NoTimewarp (b) beta-VAE (c) DMP (d) TimewarpVAE-DTW

Figure 12: Additional interpolation results

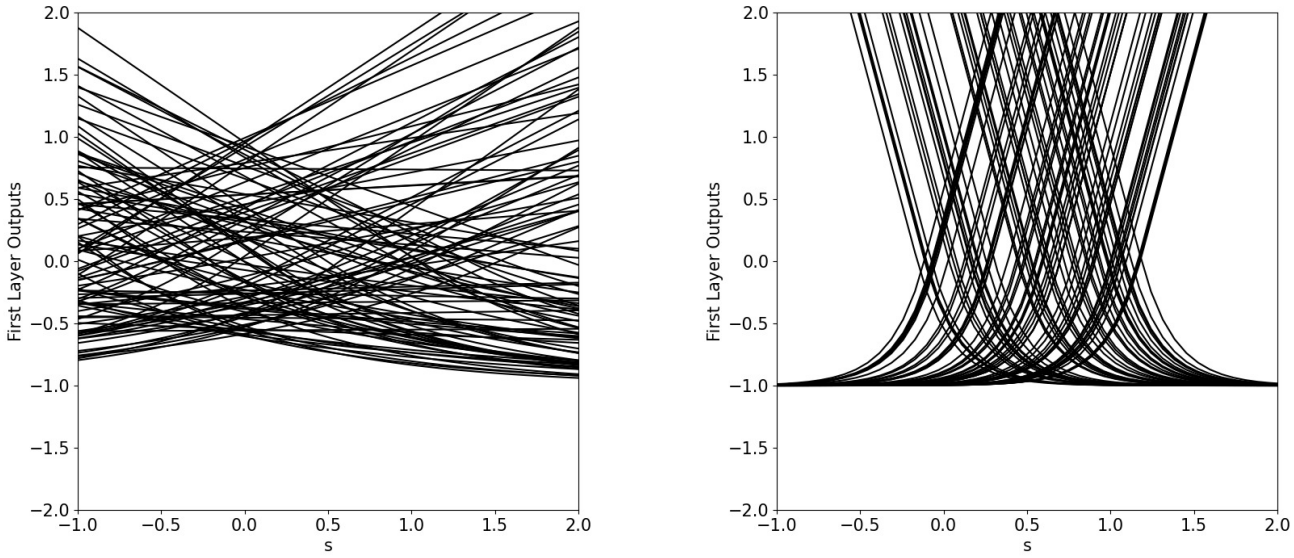

(a) Default PyTorch Initialization

(b) Custom Initialization

Figure 13: Outputs of first layer of the neural network $g(s)$.

A.8 Inspiration for Regularization Function

Our regularization function was inspired by Unbalanced Optimal Control. If we assign a uniform measure $\mathcal{U}$ to $[0, 1]$, we note that our regularization cost is exactly the symmetric KL Divergenge between $\mathcal{U}$ and the pushforward $\phi_{i*}\mathcal{U}$. For each ϕ_i, the pushforward $\phi_{i*}\mathcal{U}$ has a probability density function $1/(\phi_i'(\phi_i^{-1}(s)))$, and the symmetric KL divergence cost $D_{\mathrm{KL}}(\mathcal{U}|\phi_{i*}\mathcal{U}) + D_{\mathrm{KL}}(\phi_{i*}\mathcal{U}|\mathcal{U})$ gives the loss given above.

We work through the explicit mathematics below.

Pushforward of Probability Density Function

If F_0 is some cumulative distribution function, and F_1 is the CDF generated by the pushforward of a function ϕ then we have the simple identity $F_1(\phi(t)) = F_0(t)$. Taking the derivative of both sides with respect to t gives $F_1'(\phi(t))\phi'(t) = F_0'(t)$. The substitutions $s = \phi(t)$ and $\phi^{-1}(s) = t$ give $F_1'(s) = \frac{1}{\phi'(\phi^{-1}(s))} F_0'(\phi^{-1}(s))$. Since the PDF is the derivative of the CDF, then writing f_0 and f_1 as the corresponding PDFs of F_0 and F_1, we see

$$f_1(s) = \frac{1}{\phi'(\phi^{-1}(s))} f_0(\phi^{-1}(s)) \tag{20}$$

In the simple case where $f_0 = \mathcal{U}$, the uniform distribution over $[0, 1]$, then $f_0(t) = 1$, so we have our pushforward

$$(\phi_*\mathcal{U})(s) = \frac{1}{\phi'(\phi^{-1}(s))} \tag{21}$$

Symmetric KL Divergence Calculation

The KL divergence $D_{\mathrm{KL}}(\mathcal{U}|\phi_*\mathcal{U})$ is $\int_0^1 \log\left(\phi'(\phi^{-1}(s))\right) ds$. Substituting $\phi(t) = s$ and the corresponding $\phi'(t)dt = ds$ gives $\int_0^1 \phi'(t) \log\left(\phi'(t)\right) dt$. Likewise, the KL divergence $D_{\mathrm{KL}}(\phi_*\mathcal{U}|\mathcal{U})$ is $\int_0^1 \frac{1}{\phi'(\phi^{-1}(s))} \log\left(\frac{1}{\phi'(\phi^{-1}(s))}\right) ds$, which simplifies with the same substitutions to $-\int_0^1 \log\left(\phi'(t)\right) dt$.

The symmetric KL divergence cost is thus

$$D_{\mathrm{KL}}(\mathcal{U}|\phi_*\mathcal{U}) + D_{\mathrm{KL}}(\phi_*\mathcal{U}|\mathcal{U}) = \int_0^1 \left(\phi'(t) - 1\right) \log\left(\phi'(t)\right) dt \tag{22}$$

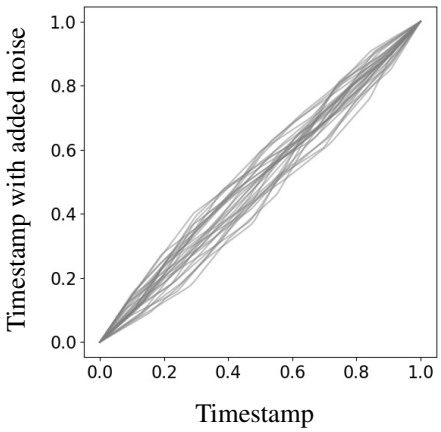

Figure 14: Example (random) functions used to add timing noise during data augmentation

A.9 Initialization of Neural Network for $f(s, z)$

As mentioned above, the neural network $f(s, z)$ is split into $\mathbf{T}(z)$ and $g(s)$. Since $g(s)$ takes in a canonical time $s \in [0, 1]$ which we want to have roughly uniform modeling capacity over the full range of s from 0 and 1, we initialize the first layer of the neural network's weights, W (a matrix with one column), and bias b (a vector) for $g(s)$ in the following way.

We initialize the values in W to be randomly, independently $-G$ or G with equal probability, where G is a hyperparameter.

We then choose values of b so that, for each (output) row j, which we denote W_j and b_j the y-intercepts of the function $y = g_j(s) = W_j s + b_j$ are each an independent uniformly random value in $[0 - \eta, 1 + \eta]$

Visually, the effect of this initialization can be seen by plotting the first layer's transformation $\mathrm{ELU}(Ws+b)$ using PyTorch's default initialization and using our proposed initialization, where ELU is the Exponential Linear Unit introduced by [Clevert *et al.*, 2016]. PyTorch's default implementation randomly initializes the output functions to be distributed symmetrically around $s = 0$. Additionally, much of the modeling capacity is assigned to variations outside the domain $[0, 1]$. Since we know that the input timestamp will be $s \in [0, 1]$, our initialization focuses the modeling capacity near $[0, 1]$ and is symmetric around the middle of that range $s = 0.5$.

A.10 TimewarpVAE Timing Noise Data Augmentation

For data augmentation of timing noise, we create perturbed timesteps to sample the training trajectories as follows. First, we construct two random vectors ν_{in} and ν_{out} of uniform random numbers between 0 and 1, each vector of length 10. We then square each of the elements in those vectors and multiply by a noise hyperparameter η and take the cumulative sum to give perturbation vectors for input and output timings. We add each of those vectors to a vector with ten elements with linear spacing, $[0, 1/9, 2/9, 3/9, \ldots, 1]$. We then normalize those perturbed vectors so that the last elements are again 1. The resulting vectors now give nicely symmetric, monotonic x and y coordinates of knots for a stepwise-linear perturbation vector which we can subsample at arbitrary timesteps to give desired noise-added output timesteps. We choose $\eta = 0.1$ in our experiments, giving noise functions plotted in Fig. 14.

When using this data augmentation, each time we pass a training trajectory into our model, instead of sampling the training trajectory at T uniformly-distributed timesteps between 0 and 1 to construct our $x \in \mathbb{R}^{T \times n}$, we first perturb all those timesteps by passing them through a randomly generated noise functions. This means that each x we pass into our learning algorithm has a slightly different timing than the training data, allowing us to perform data augmentation on the timings of the training data.

A.11 Alternative TimewarpVAE Approach Directly Using Dynamic Time Warping

An alternative formulation of TimewarpVAE, which we call TimewarpVAE-DTW, is to collect the decoded trajectory as a vector by running the decoder $f(s, z)$ over multiple, evenly-sampled canonical timesteps s, and then warping those generated timesteps to the training data using DTW. This is more similar to Rate Invariant AE, in that the time-warping happens after trajectory generation, however, we do not require linear interpolation. Instead, we convert the DTW alignment into a loss in such a way that all canonical trajectory points are used and averaged (using the same weightings we descriped for our Aligned RMSE). This avoids the problem encountered in Rate Invariant AE where parts of the canonical trajectory can be completely ignored. TimewarpVAE-DTW requires running DTW to align each reconstructed trajectory to its associated training trajectory every time the decoder function is executed during training. This is significantly less efficient than our suggested implementation of TimewarpVAE, because it requires many executions of dynamic time warping with no re-use of the DTW results between

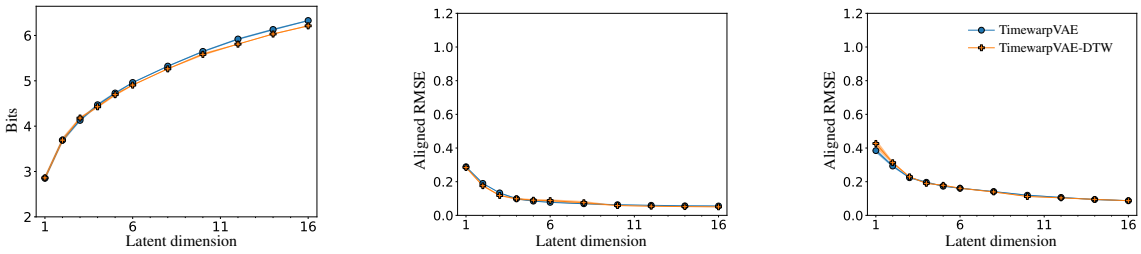

(a) Rate (b) Train Distortion (c) Test Distortion

Figure 15: Performance comparison between TimewarpVAE and TimewarpVAE-DTW

Table 2: Hyperparameters

Name	e conv channels strides	h conv channels strides	$g(s)$ fc	$\mathbf{T}(z)$ fc	f fc conv channels
TimewarpVAE	[16,32,64,32] [1,2,2,2]	[16,32,32,64,64,64] [1,2,1,2,1,2]	[500,500]	[200]	–
NoTimewarp	[16,32,64,32] [1,2,2,2]	–	[500,500]	[200]	–
NoNonlinearity	[16,32,64,32] [1,2,2,2]	[16,32,32,64,64,64] [1,2,1,2,1,2]	[500,500]	[]	–
beta-VAE	[16,32,64,32] [1,2,2,2]	–	–	–	[800] [20,20,n]
Rate Invariant AE	[32,32,32] [1,1,1]	–	–	–	[6400] [32,32,n]

training steps. Our suggested implementation, TimewarpVAE, explicitly models the time-warping, so is able to re-use (and update) the warping function between steps, rather than recalculating it from scratch each time. However, we note in Fig.15 that TimewarpVAE-DTW, though less efficient, can give comparable results. In this implementation we use DTW, but a Soft-DTW [Cuturi and Blondel, 2017] could be used instead.

A.12 Hyperparameters

The specific training architectures we use is shown in Table 2. We use a kernel size of 3 for all convolutions. e is the spatial encoding architecture (which is always reshaped to a vector and followed by two separate fully connected layers, one outputting the expected encoding, and one outputting the log of the diagonal of the covariance noise). h is the temporal encoding architecture, which is always followed by a fully connected layer outputting a vector of size $K = 50$. $g(s)$ is part of the factorized decoder architecture, which is followed by a fully connected layer outputing a vector of size $m = 64$. $\mathbf{T}(z)$ is the other part of the factorized decoder architecture, which is followed by a fully connected layer outputting a vector of size nm where n is the number of channels in the training data (2 for handwriting, 7 for fork trajectories) and $m = 64$. For beta-VAE, instead of the factorized decoder architecture, we use one fully connected layer with output size 800, which we then reshape to size 25×32. This is followed by one-dimensional convolutions. Following the approach of [Kuester *et al.*, 2021], for the convolutions in the beta-VAE architecture, instead of doing convolutional transposes with strides to upsample the data, we instead always use a stride length of 1 and upsample the data by duplicating each element before performing each convolution. Thus, the lengths expand from 25 in the input to the output size of 200 after the three convolutions.

We use a learning rate of 0.0001, a batch size of 64, and a rectified linear unit (ReLU) for all spatial and temporal encoder nonlinearities, except for Rate Invariant AE for which follow the literature and we use Tanh. We use an exponential linear unit (ELU) for the decoder nonlinearities for TimewarpVAE, we use ReLU for the decoder nonlinearities for beta-VAE, and we again use Tanh for the Rate Invariant AE. We choose a variance estimate of $\sigma_R^2 = 0.01$ for our data, but this hyperparameter is not critical, as it is equivalent to scaling β and λ in our TimewarpVAE objective. In order to compute the Rate (information bottleneck) of the Rate Invariant AE, we implement it as a VAE instead of an autoencoder, only adding noise to the spatial latent, not to the timing latent values. We use 199 latent variables for the timing (one fewer than the trajectory length), and vary the number of spatial latent variables.

A.13 Robot Execution

Here we give specifics on the execution of the TimewarpVAE trajectory on the Kinova Gen3 robot arm.

Optimization Formulation

We formulate an optimization problem to find the fastest feasible trajectory that satisfies the joint speed an torque constraints of our Kinova Gen3 robot arm and follows the training demonstration trajectory within a defined time-warping cost. We use Drake [Tedrake and the Drake Development Team, 2019] to efficiently formulate several of the constraints, including the forward dynamics of the manipulator arm.

We write the time-warping function ϕ now as a function from real time $[0, T]$ to canonical time $[0, 1]$. Given the target canonical path $p(s) : [0, 1] \to \mathbb{R}^3$, and our robot joints as a function of the real time $j(t) : [0, T] \to \mathbb{R}^7$ and our forward robot kinematics mapping joint angles to end-effector position $f(j) : \mathbb{R}^7 \to \mathbb{R}^3$. Our first constraint is that the robot must follow the canonical path according to the time-warping funciton

$$p(\phi(t)) = f(j(t)) \tag{23}$$

We also constrain the time-warping function ϕ to be monotonically positive from $[0, T]$ to $[0, 1]$ by constraining its slope to be positive and for ϕ to have the right boundary constraints:

$$\phi'(t) > 0 \tag{24}$$

$$\phi(0) = 0 \tag{25}$$

$$\phi(T) = 1 \tag{26}$$

We define the forward kinematics funciton f by loading the Kinova Gen3 URDF into Drake. Likewise, we model the forward dynamics using drake, so that, under input joint torques at time $t$given by $\tau(t) : [0, T] \to \mathbb{R}^7$ we know the joint accelerations $j''(t)$ as a funciton of time. The forward dynamics gives us a differential equation of $j''(t)$ as a funciton of j', j, and τ. Using FD as the forward dynamics function, we have the constraint

$$j''(t) = FD(j'(t), j(t), \tau(t)) \tag{27}$$

We additionally add joint speed limits $j'_{i\text{max}}$ for each joint i.

$$-j'_{i\text{max}} \leq j'_i(t) \leq j'_{i\text{max}} \tag{28}$$

We also add torque constraints for each joint i

$$-\tau_{i\text{max}} \leq \tau_i(t) \leq \tau_{i\text{max}} \tag{29}$$

Finally, we add a time-warping constraint, that our time-warping regularization value must be less than some bound. We note that we adjust the definition of our time-warping cost to account for the new domain of the time-warping of $[0, T]$ instead of $[0, 1]$. Our time-warping regularization value now contains additional factors of T and $\frac{1}{T}$ so that it is not affected by linear scaling of the real time duration T.

$$\frac{1}{T}\int_0^T (T\phi'(t) - 1)\log(T\phi'(t))\, dt \tag{30}$$

and we constrain this to be below some value C_{warp}

$$\frac{1}{T}\int_0^T (T\phi'(t) - 1)\log(T\phi'(t))\, dt \leq C_{\text{warp}} \tag{31}$$

Our optimization objective is to minimize T (how long it takes the robot to perform the motion) subject to all the constraints above.

Optimization Using Direct Collocation

To numerically solve the optimization problem, we use the direct collocation appraoch of [Hargraves and Paris, 1987] implemented in Drake. Rather than requiring that all the constraints above be satisfies at all timesteps, we only check constraints at fixed, equally-spaced timesteps. In particular, we approximate $j(t)$,$j'(t)$,and $\phi(t)$ as cubic splines (with K segments) and $K + 1$ equally spaced knots (including the knots at the endpoints at 0 and T), and we constrain the derivative of the cubic spline $j(t)$ to equal the cubic spline $j'(t)$ at the knot and at the collocation points (which are the midpoints in between two knots). We restrict $\tau(t)$ and $\phi'(t)$ to be piecewise affine with the same equally-spaced knots, and we now just check the following constraints at knot points and collocation points:

$$p(\phi(t)) = f(j(t)) \tag{32}$$

$$-j'_{i\text{max}} \leq j'_i(t) \leq j'_{i\text{max}} \tag{33}$$

$$-\tau_{i\text{max}} \leq \tau_i(t) \leq \tau_{i\text{max}} \tag{34}$$

$$j''(t) = FD(j'(t), j(t), \tau(t)) \tag{35}$$

The following constraints are only checked at knot points:

$$\phi'(t) > 0 \tag{36}$$

And, of course, the following constraints are still just at the boundary points:

$$\phi(0) = 0 \tag{37}$$

$$\phi(T) = 1 \tag{38}$$

The warping cost constraint is now approximated by a trapizoidal integration over the $K+1$ knot points $t_k \in \{0, \ldots, T\}$:

$$\sum_{t_k} w_k \left(T\phi'(t_k) - 1\right) \log(T\phi'(t_k)) \leq C_{\text{warp}} \tag{39}$$

where the weighting w_k is $\frac{1}{2K}$ if t_k is 0 or T (a boundary) and $\frac{1}{K}$ otherwise.

We then optimize using IPOPT [Wächter and Biegler, 2005], terminatng after 2000 max iterations. We use $K = 20$ cubic spline segments. For NoWarping, we set the max time-warping cost C_{warp} to zero, and when we allow warping, we set the max time-warping allowed to 0.05. Based on the Kortex Gen3 User Guide, we set the joint speed limits to 1.39 rad/s for the first four joints and 1.22 rad/s for the last three joints. Likewise, we set the joint torque limits to 32 Nm for the first four joints and 13 Nm for the last three joints.

Robot Control

For robot execution, we send low-level joint commands at 500Hz to the Kinova Gen3 arm, using a PID controller to follow the desired joint position and velocities. The low-level commands directly specify the current desired for each joint, since we found there to be an unusably high delay when commanding via the TORQUE_HIGH_VELOCITY low-level API provided by Kinova, leading to controller instability. The TORQUE low-level API is implemented by Kinova leads to stable control, but contains a cascading controller that includes a velocity control loop, and therefore does not match the expected relationship between commanded torque and joint accellerations (in particular, commanding a robot joint to move with maximal torque accelerates the joint much more slowly than it would without Kinova's cascading controller). For these reasons, we use the MOTOR_CURRENT low-level API in a PID loop to command the Kinova Gen3 arm to track the joint trajectory returned from our optimization calculation.